5th International Conference on Experimental Fluid Mechanics ICEFM 2018 Munich
Munich, Germany, July 2-4, 2018

Influence of leading edge tripping devices on supersonic turbulent boundary layer characteristics

Matthew Bross[1*], Sven Scharnowski[1], Christian J. Kähler[1]

[1] Universität der Bundeswehr München,
Institute of Fluid Mechanics and Aerodynamics, Neubiberg, Germany

[*] matthew.bross@unibw.de

Abstract

In this investigation, the influence of well known tripping devices on a zero pressure gradient (ZPG) compressible turbulent boundary layer at a supersonic Mach number is considered. Measurements are performed on a flat plate model with a sharp leading-edge in the Trisonic Wind Tunnel Munich (TWM) at Ma = 2.0 and friction Reynolds number in the range $Re_\tau = 5000-6000$. Velocity fields are recorded using stereoscopic particle image velocimetry in the wall-normal spanwise (yz) plane. The location of the transition line with and without tripping was estimated using oil-film visualization. It was demonstrated that zag tape, dot pattern, and solid stripes generate specific coherent vortex patterns in the near wall flow field but they seem to have little measurable effect on the mean velocity profile and boundary layer thickness. However, the streamwise and wall normal Reynolds stress components appear influenced by these devices in the outer field due to the near wall disturbances in the wake of the tripping devices.

1 Introduction

Transitional devices at the leading edge of aerodynamic surface are commonly used to ensure laminar/turbulent transition or to fix the transition location. However, these devices can produce unwanted flow features such as longitudinal vortices or blockage that can influence coherent flow structures in turbulent boundary layer and condition the results of a measurement if an inadequate transition or perturbation is selected (Hutchins, 2012).

The influence of tripping devices on a developing flat plat turbulent boundary layer was recently studied experimentally at large Reynolds numbers ($Re_\theta = 7200-34900$) by Marusic et al. (2015). They tested sandpaper, and two different diameter threaded rods. Marusic et al. (2015) conclude that the devices produce measurable effects in the mean flow, Reynolds stress, and spectra. For the over-tripped case the effects could persist to 2000 trip heights. Furthermore, even for more moderate tripping, the emergence of an artificial outer peak in the spectra at lower Reynolds numbers than expected was observed. Consistent with the aformentioned study, Rodríguez-López et al. (2016) tested cylindrical and saw shaped disturbances in order to greatly thicken the boundary layer and thereby increase the Reynolds number. While these devices were successful in thickening the boundary layer, depending on the blockage ratio of the tripping configuration, non-canonical boundary layers were generated even after long distances downstream (100-150 trip heights) from the tripping device.

The influence of commonly used zig-zag tape was investigate experimentally at low Reynolds number by Elsinga and Westerweel (2012). The results reveal the presence of undulating voritices downstream of the trip and where shown to have a signature in coherent structures up to 28 boundary layer thickness downstream. Extending to larger Reynolds numbers, Sanmiguel Vila et al. (2017) tested various V and zig-zag like tripping devices on a ZPG turbulent boundary layer (up to $Re_\theta = 4000$). They show that even weak tripping can lead to deviations in the mean velocity field and strong trips produce amplified secondary velocity fluctuations in the outer region.

Much less examined is the effect of tripping devices on supersonic turbulent boundary layers. To fill the gap, the purpose of the experiment presented herein is to study the effect of tripping devices on supersonic flow where the boundary layer is often very thin and thickening by means of transition device is beneficial from an experimental point of view in order to resolve the flow better.

2 Experiment Description

2.1 Trisonic Wind Tunnel Munich

The Trisonic Wind Tunnel Munich (TWM) is a blow-down type wind tunnel with a 300 mm $\times$ 675 mm (w $\times$ h) test section. A two-through system consisting of an adjustable Laval nozzle and an adjustable diffuser allows for a stable operating Mach number range from 0.2 to 3.0. The stagnation pressure is controlled by a pressure regulation value and is adjustable between $p_0 = 1.2\,\text{bar}$ and $5.0\,\text{bar}$. This allows to set the Reynolds number independently of the Mach number. The corresponding Reynolds number range is $(4-80)\times 10^6\,\text{m}^{-1}$. Reynolds number and Mach number can be varied during the wind tunnel run. The facility has two holding tanks that can be pressurized up to 20 bar above ambient pressure, with each tank holding a volume of 178 m^3 of air. This amount of air is sufficient for run times in the order of 100 seconds for the cases discussed below. The wind tunnel's test section is enclosed by a plenum chamber and also has the ability to apply boundary layer suction at both the vertical and the horizontal walls independently. Figure 1 gives an overview of the wind tunnel.

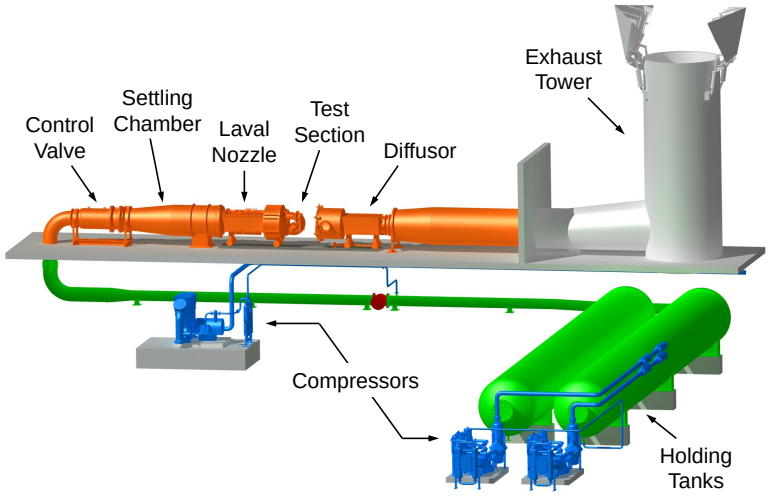

Figure 1: Trisonic Wind Tunnel Munich overview.

2.2 Flat Plate Boundary Layer Model and Tripping Devices

A flat plate boundary layer model was mounted in the test section of the TWM for this investigation. A sketch of the model and coordinate system is shown in Figure 2(a). The overall length of the model in the streamwise direction is 750 mm, resulting in a turbulent boundary layer thickness of around 4−5 mm at the measurement location 375 mm downstream of the leading edge. The leading-edge of the plate was sharpened to ensure that an attached shock forms on the leading-edge during supersonic inflow conditions.

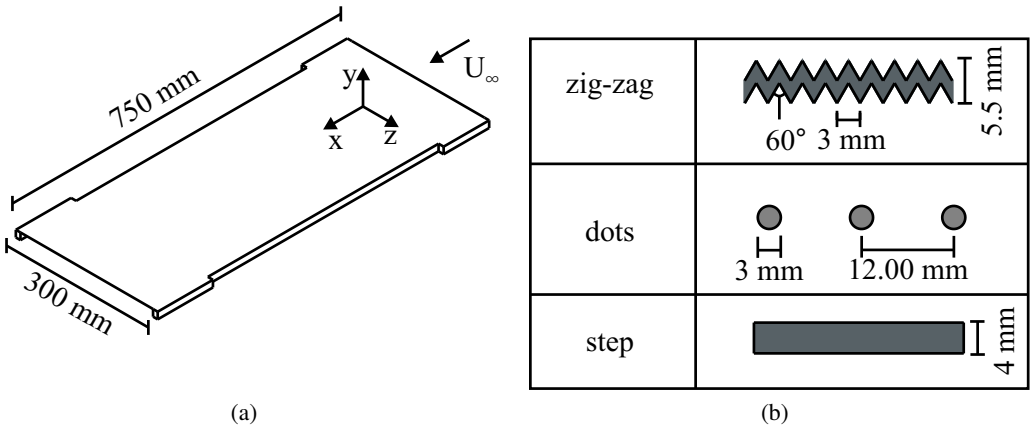

Figure 2: (a) Flat plate model used for investigation. (b) Tripping devices used, all with thickness 60μm.

Several tripping designs where tested in this investigation, which are representative of commonly used devices throughout associated literature. The details of the zig-zag, distributed dots, and single stripe tripping devices are shown in Figure 2(b). The tripping devices were custom printed on double sided tape so that they can be easily applied and removed from the flat plate boundary layer model. The laminar boundary layer thickness was estimated from the Blasius solution making the 60μm thick tripping devices round $0.5-0.7\delta_{99L}$.

3 Oil Film Visualization

Oil film techniques were used to visualize the influence of the tripping devices on the transition process in the near field. This technique it was possible to estimate the natural transition location and the footprint of the wake, on the wall for the three transition devices described in figure 2(b).

A film of an oil mixture, consisting of petroleum oil, linseed oil, Oleic acid and TiO_2 particles, was applied to the plate in a homogeneous manner by using a industrial paint sprayer device before each wind tunnel run. The plate surface was black anodized Aluminum which allowed for better contrast. The oil film streaks then were captured with two side by side cameras, creating a field of view that spans the entire test section width. The plate was illuminated with a white LED diffuse light source in order to create sufficient contrast.

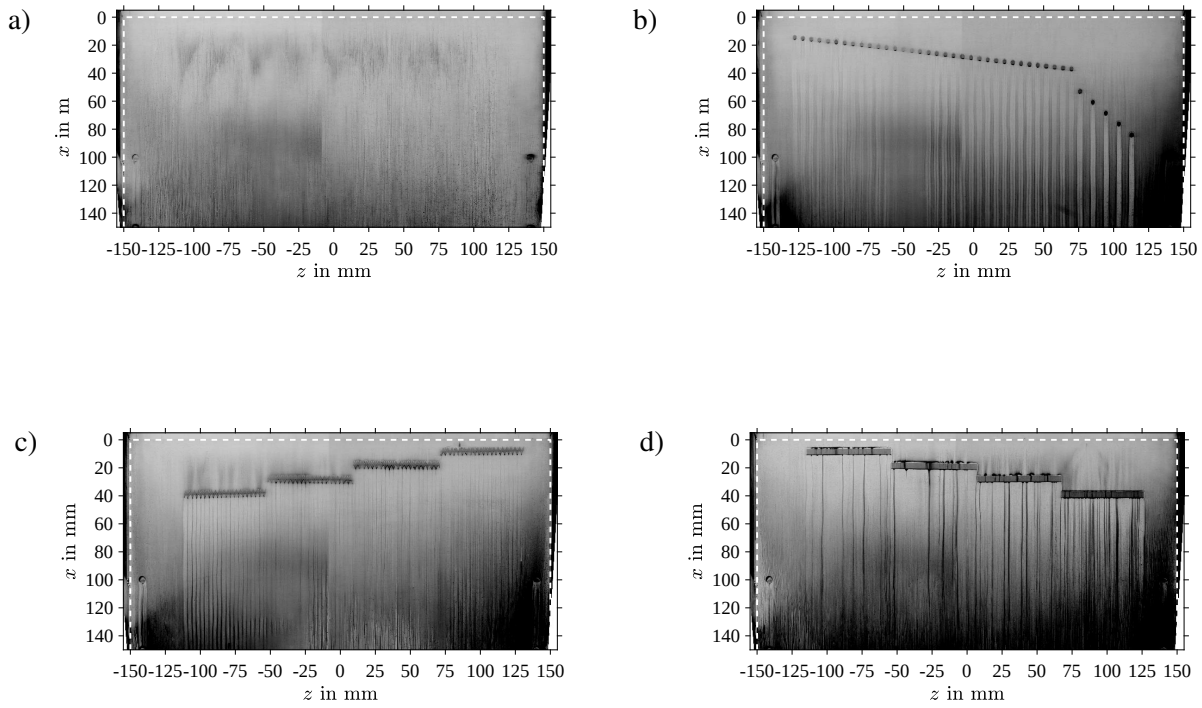

Figure 3: Stitched side by side images of oil film visualization at Ma = 2.0 for (a) Clean (b) Dots (c) zig-zag tape and (d) rectangular strip. Flow direction is from the top to bottom (x-direction).

Oil streak patterns at Ma = 2 for the clean, dots, zig-zag, and stripe cases are shown on figure 3(a-d), respectively. The field of view shown here is created by stitching together both cameras so that the full width (spanwise direction) of the test section becomes visible. From the clean case, figure 3(a), the natural, i.e. unforced, transition location can be estimated by observing the transition wedge pattern near the leading edge. Transition wedges can only be observed where the flow is still laminar. Therefore, the transition location appears to be between 25 and 30 mm downstream of the leading-edge.

Keeping this in mind, transition devices were placed at different streamwise locations, before, at, and after the transition location that was observed in the clean case. The oil streaks for these cases are shown in figure 3(b-d). For each transition device, a long wake downstream of the tripping devices is present, even if the tripping device is placed after the natural transition location. Especially for the dots and zig-zag patterns this wake indicates the existence of high coherent counter rotating streamwise vorticies that persist over the full field of view. Furthermore, it can be seen that the coherent vortex pattern is always generated no matter which location the tripping was placed. Therefore, the tripping configuration for the following analysis consists of one straight line of tripping across the entire spanwise direction of the plate, 30 mm downstream of the leading-edge.

4 Stereo Particle Image Velocimetry

In order to examine if the coherent vortices/wakes influence the statistical properties of turbulent boundary layer much further downstream of the leading edge, beyond thickening the boundary layer, quantitative measurements by means of particle image velocimetry were performed. Stereo particle image velocimetry (SPIV) measurements were performed in a yz-plane (wall-normal spanwise) approximately 375 mm downstream of the leading-edge or 6250 tripping step heights. In this case the out-of-plane component is the streamwise direction. This SPIV orientation was selected in order to observe the height and spacing of ve-

locity structures in the wall-normal and spanwise directions while at the same time recording information about the streamwise velocity component.

In order to perform quantitative flow visualization, a global seeding system introduced tracer particles upstream of the test section. DEHS oil particles are produced by a conventional impactor seeding generator that creates particles with an approximately 1 μm mean diameter. The tracer particles in the test section were illuminated in a spanwise-wall normal plane by a double pulse laser system (Evergreen Quantel) with maximum pulse energy of 200 mJ at 15 Hz and 532 μm wavelength. The light sheet thickness was around $1-2$ mm.

Particle images were recorded on two 5.5MP CMOS cameras (Imager sCMOS, PCO GmbH, LaVision). Using 100 mm/f2.8 Zeiss objectives and Scheimpflug mounts, the resulting scaling in the center of the FOV was $\sim$12.9 μm/pix. By dividing the pixel pitch of the sCMOS camera (6.5 μm/pix) the resulting magnification in the center of the FOV was $M = 0.5$, corresponding to a field of view of 25×53 mm^2. The associated imaging parameters are listed in Table 1.

Table 1: Imaging parameters for Stereo PIV

Parameter			**Stereo-PIV**
recording rate	f	[Hz]	15
scaling factor	m	[μm/pix]	12.9
magnification	M		0.5
field of view, (FOV)	y,z	[mm^2]	53×23
Number of samples			1000

Three-component vector fields were calculated by reconstructing the stereo images and using standard multi-pass PIV algorithm including iterative image deformation and Gaussian window weighting. Care is taken to filter outliers and remove spurious vectors. Finally for the mean profiles, a histogram of the velocity fluctuations was computed for each wall normal position and fit with a Gaussian function to ensure the final mean value is not biased by remaining outliers.

4.1 Mean Velocity Profiles

Streamwise mean velocity profiles were calculated and fit using the classical "Law of the Wall" plus the Coles wake correction shown in equation (1). In this case the values κ and C were set to 0.41 and 5.2 respectively.

$$u = \frac{1}{\kappa}\log\left(\frac{u_\tau y}{\nu}\right) + C + \frac{2\Pi}{\kappa}\sin^2\left(\frac{\pi}{2}\frac{y}{\delta_c}\right) \tag{1}$$

Since the near wall region was not resolved in this measurement the near wall parameters such as u_τ are calculated from fitting the data to equation 1. The wall position was determined with sub-pixel resolution by iteratively shifting the y-position of the velocity profile and selecting the shift that best match the profile to equation 1. The resulting mean streamwise velocity profiles are shown in figure 4 for the clean, dots, zig-zag, and stripe tripping case. The boundary layer parameters calculated from these profiles are summarized in table 2. Looking at the mean velocity profile, it appears that boundary layer parameters do not change significantly between tripping and the clean case.

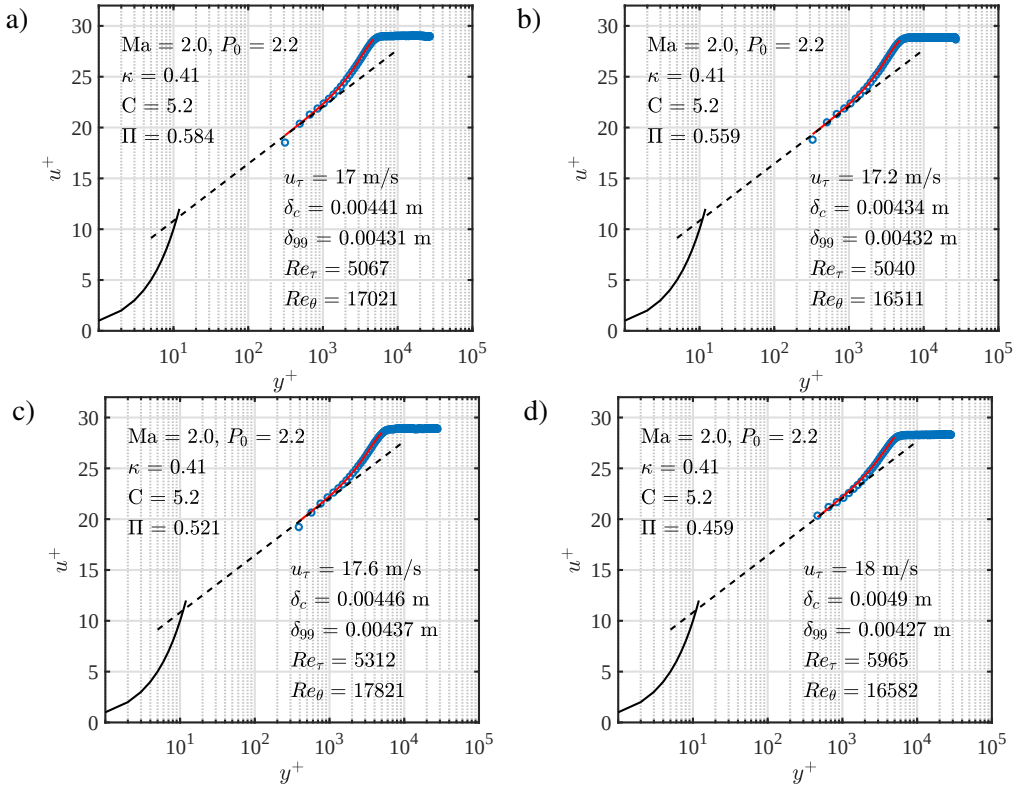

Figure 4: Mean streamwise velocity profiles at Ma = 2.0 for (a) Clean (b) Dots (c) Zig-zag (d) Stripe cases. Vector fields generated from 24 by 24 pixel^2 PIV windows.

Table 2: Boundary Layer Parameters for Ma = 2.0 p_0 = 2.2 bar

Parameter		**Clean**	**Dots**	**Zig-zag**	**Stripe**
δ_{99}	[mm]	4.31	4.32	4.37	4.27
δ_c	[mm]	4.41	4.34	4.46	4.90
u_τ	[m/s]	17.0	17.2	17.6	18.0
Re_θ	[−]	17021	16511	17821	16582
Re_τ	[−]	5067	5040	5312	5965

4.2 Reynolds Stresses

While the mean streamwise velocity profiles shown in figure 4 appear to show little difference between clean and tripping cases it is important to also look at the fluctuation fields. In figure 5 the streamwise $\langle u'u' \rangle$ and wall-normal $\langle v'v' \rangle$ stresses are shown for the clean and all of the tripping cases. The stresses are normalized with u_τ^2 and both inner and out wall normal scaling are shown on the top and bottom horizontal axis, i.e. y^+ and y/δ_{99}. All values were calculated with 24 by 24 pixel^2 interrogation window.

Consistent with previous studies for incompressible flow a broadening of the Reynolds stresses appears when using tripping devices. In figure 5(a) the $\langle u'u' \rangle$ stresses for the tripped cases are larger in the outer region. Furthermore, the shape of the stripe profile (green) appears the most different. The zig-zag tape, which is expected to produce streamwise oriented vortices, seems to increase the $\langle u'u' \rangle$ and $\langle v'v' \rangle$ values as well. It should be mentioned that the Reynolds stresses plotted in figure 5 do not all converge to the same

value once δ is reached. This could be for several reasons including measurement errors and lack of spatial resolution. However, in the blow down facility that the measurements have been conducted, the turbulence intensity is around 0.75% (Scharnowski et al., 2018) for the Mach number tested. This is much larger than conventional wind tunnels and could as well contribute to the discrepancy in the fluctuations recorded in the freestream.

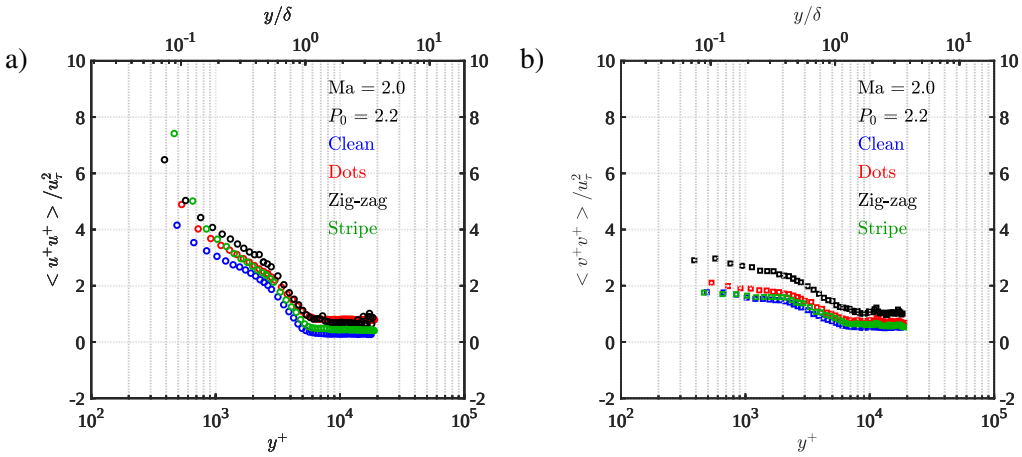

Figure 5: Ma = 2.0 Reynolds Stresses for (a) $\langle u'u' \rangle$ (b) $\langle v'v' \rangle$ for all tripping cases. Vector fields generated from 24 by 24 pixel^2 PIV windows. Both inner and out wall normal scaling are shown on the top and bottom horizontal axis, i.e. y^+ and y/δ_{99}.

5 Conclusion

A compressible Ma = 2.0 turbulent boundary layer at high Reynolds numbers was investigated with oil flow visualization and SPIV measurements to determine the influence of commonly used leading-edge tripping devices on the boundary layer mean velocity field and Reynolds stresses. Along with the clean case, tripping devices consisting of spherical dots, zig-zag tape, and solid stripe were considered. The trip height was selected so that the boundary layer was minimally or at most moderately tripped.

It was observed in all tripping cases that long wake persists along the surface of the plate, and it must be expected that they influence the near wall flow features. For both the dots and zig-zag patterns, wake patters evident of strong longitudinal voritices were present. However, the tripping's influence on the outer region of the boundary layer is negligible as demonstrated by stereo particle image velocimetry measurements in a spanwise wall normal plane approximately 6250 trip heights downstream from the leading-edge. At this location the wall-normal streamwise velocity profile did not indicate any large difference between the clean and tripped cases. Most notable, the boundary layer thickness did not change.

However, the Reynolds stresses profiles show some spreading between the clean and tripped cases even in the outer region of the boundary layer. The zig-zag and stripe tape produced the most difference between the clean case for both $\langle u'u' \rangle$ and $\langle v'v' \rangle$. However an open question remains as to why the freestream fluctuations do not converge in the freestream for all the tripping cases tested. Disturbances due to the small tripping devices that propagate towards in the freestream region, causing slightly enhanced velocity fluctuations is one possible explanation. However, measurement uncertainty and the wind tunnel turbulence level also play a role. Nerveless, this the Reynolds stress levels suggest that there is some extra turbulent energy in the outer region of the boundary layer induced by the tripping devices, even several thousand trip heights downstream. This is important because it shows that small near wall disturbances can alter the turbulent flow structures in the outer region.

Acknowledgements

This work is supported by the Priority Programme SPP 1881 Turbulent Superstructures funded by the Deutsche Forschungsgemeinschaft project number KA1808/21-1.

References

Elsinga GE and Westerweel J (2012) Tomographic-piv measurement of the flow around a zigzag boundary layer trip. *Exp in Fluids* 52:865–876

Hutchins N (2012) Caution: tripping hazards. *J Fluid Mech* 710:14

Marusic I, Chauhan KA, Kulandaivelu V, and Hutchins N (2015) Evolution of zero-pressure-gradient boundary layers from different tripping conditions. *J Fluid Mech* 783:379411

Rodríguez-López E, Bruce PJK, and Buxton ORH (2016) On the formation mechanisms of artificially generated high reynolds number turbulent boundary layers. *Boundary-Layer Meteorology* 160:201–224

Sanmiguel Vila C, Vinuesa R, Discetti S, Ianiro A, Schlatter P, and Örlü R (2017) On the identification of well-behaved turbulent boundary layers. *J Fluid Mech* 822:109138

Scharnowski S, Bross M, and Kähler CJ (2018) Estimating wind tunnel turbulence level by means of PIV/PTV . in *Fachtagung Experimentelle Strömungsmechanik, Sept. 4-6, Rostock, Germany*